arXiv:1304.7511v1 [cond-mat.mes-hall] 28 Apr 2013

Extrinsic spin Hall effect in graphene

Aires Ferreira[1], Tatiana G. Rappoport[2], Miguel A. Cazalilla[1], and Antonio H. Castro Neto[1,3]
[1]*Graphene Research Centre and Department of Physics,*
National University of Singapore, 2 Science Drive 3, Singapore 117546.
[2]*Instituto de Física, Universidade Federal do Rio de Janeiro,*
CP 68.528, 21941-972 Rio de Janeiro RJ, Brazil. and
[3]*Department of Physics, Boston University, 590 Commonwealth Avenue, Boston, MA 02215, USA.*

We show that extrinsic spin Hall effect can be engineered in monolayer graphene by decoration with small doses of adatoms, molecules or nano-particles originating local spin-orbit perturbations. The analysis of the single impurity scattering problem shows that intrinsic and Rashba spin-orbit local couplings enhance the spin Hall effect via skew scattering of charge carriers in the resonant regime. The solution of the transport equations for a random ensemble of spin-orbit impurities discloses that giant spin Hall currents are within the reach of current state-of-the-art in device fabrication. The spin Hall effect is robust with respect to thermal fluctuations and disorder averaging.

PACS numbers: 71.27.+a,73.20.Hb,75.30.Hx

The spin Hall effect (SHE) [1–4], that is, the appearance of a transverse spin current in a non-magnetic conductor by pure electrical control has been predicted to occur in materials with large spin-orbit interaction (SOI). Over the last decade, its study has lead to an intense experimental activity [5–9], due to its potential application in spintronics. Recently, the SHE has been explored for replacing ferromagnetic metals with spin injectors in applications [10, 11], opening the doors to the development of spintronic devices without magnetic components.

The activation and control of spin-polarized currents in solid-state is both of fundamental and technological interest. SHEs could be used for an efficient conversion of charge current into spin-polarized currents. The ratio of the spin Hall current to the steady-state charge current, commonly known as the spin Hall angle θ_{sH}, measures this efficiency and it is the most important figure of merit for practical applications. Broadly speaking, SHEs in metals and semiconductors originate from (i) *extrinsic* mechanisms, which are due to spin-dependent scattering of electrons by impurities in the presence of SOI [1–3], and (ii) *intrinsic* mechanisms, entirely due to SOI in the electronic band and that occur in the absence of any scattering process. In semiconductors, the spin Hall angles are in the range of $0.0001 - 0.001$ [5, 7]. On the other hand, the experimental values of θ_{sH} for metals can be considerable larger, being of the order of 0.01 for Pt [12] and 0.1 in a recent measurement performed in Ta [11].

After its successful isolation, graphene [13] has also become the subject of intensive study in spintronics [14–18]. In this material, electrons can propagate ballistically and carrier density and carrier polarity can be controlled by an external gate. Spin-orbit and hyperfine interactions are extremely weak in graphene, and therefore the spin coherence length is expected to be long [19, 20]. These characteristics make graphene appealing for *passive* spintronic applications e.g., as a high-fidelity channel for spin-encoded information [21]. One striking possibility is to manipulate electronic properties of graphene for *active* spintronics. This may be achieved via spin-orbit splitting of the band dispersion e.g., by bringing heavy metallic atoms in close contact to graphene [22], or by locally inducing sizable SOI (~ 10 meV) [23, 24]; in Ref. [23], distortions induced by covalently bonded impurities were predicted to produce the desired effect, and Ref. [24] suggests local SOI enhancement via tunneling of electrons in and out a heavy atom. Moreover, it has been proposed that, in the presence of SOI, graphene could exhibit the quantum spin Hall effect [25].

In this Letter, we consider a monolayer of graphene decorated by a small density of impurities generating a spin-orbit interaction in their surroundings. We show that robust SHEs develop through asymmetric (*skew*) scattering events. Crucially, and unlike two-dimensional electron gases (2DEG), for which resonant enhancement of skew scattering [26] requires resorting to fine tuning and sometimes to exotic phenomena such as the Kondo effect [27, 28], our proposal takes advantage of graphene being a atomically thin membrane, whose local density of states easily resonates with several types of adatoms, molecules, or nano-particles. Resonant scatterers have been predicted to play an important role in charge transport at high electronic densities [29, 30]. Here, we argue that a similar physics is behind a huge potential of graphene for extrinsic SHEs. The decoration with small doses of adatoms/nano-particles only partially suppresses the charge carrier mobilities of graphene devices, which combined with large spin diffusion lengths and Fermi energy tunability, makes this material a promising candidate for spintronic integrated circuits with SHE-based spin-polarized current activation and control.

According to our calculations, extrinsic spin Hall effect in graphene, as that recently reported in hydrogenated graphene [31], can originate from skew scattering alone. The latter is absent in the first Born approximation [32], and therefore we compute transport relaxation rates non-

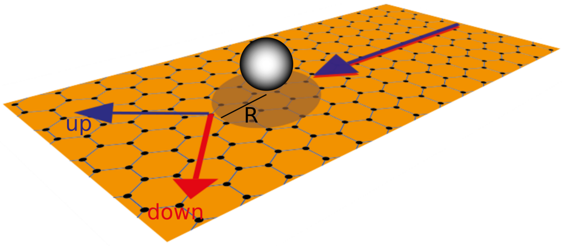

FIG. 1: Schematic picture of extrinsic spin Hall effect generated by transport skewness. An impurity (sphere) near the graphene sheet causes a local spin-orbit field with range R. The scattering of components with positive (negative) angular momentum is enhanced (suppressed) for charge carriers with $s_z = 1$ ($s_z = -1$), resulting in a net spin Hall current.

perturbatively via exact partial-waves expansions. We predict that clustering of adatoms or nano-particles leads to an enhancement of the spin Hall angle comparable to those found in pure metals ($\theta_{\mathrm{sH}} \sim 0.01 - 0.1$ [5, 7, 12]).

In order to study the amount of extrinsically generated SHE and its dependence on impurity type, Fermi energy and temperature, we consider a continuum model of graphene decorated with a small concentration of local SOI impurities with different symmetries (see later). The starting point is the continuum-limit Hamiltonian of graphene $\mathcal{H}_0 = \hbar v_F(\tau_z\sigma_x p_x + \sigma_y p_y)$, where $\mathbf{p} = (p_x, p_y)$ is the 2D kinematic momentum operator around one of the two inequivalent Dirac points (K and K'), $v_F \approx 10^6$ m/s is the Fermi velocity, $\boldsymbol{\sigma}$ and $\boldsymbol{\tau}$ denote Pauli matrices, with $\sigma_z = \pm 1$ [$\tau_z = \pm 1$] describing states on A(B) sublattice [at $K(K')$]. The spin-orbit splitting in the band structure of pristine graphene is of the order of 10 μeV and therefore can be safely neglected [20]. The impurities play the role of scattering centers that locally induce SOI of the intrinsic type $\mathcal{V}_{\mathrm{SO}} = \Delta_I(\mathbf{r})\tau_z\sigma_z s_z$ and/or Rashba-type $\mathcal{V}_{\mathrm{SO}} = \Delta_R(\mathbf{r})(\tau_z\sigma_x s_y - \sigma_y s_x)$ (here $\mathbf{s}$ are Pauli matrices for spin). In addition, they also induce a spin-independent electrostatic potential $V(\mathbf{r})$ which accounts for extra scalar scattering. However, adatoms on graphene often tend to cluster due to ripples (as it is the case of H [33]) or due to a low absorption energy [34]. In such cases, the intervalley scattering can be neglected and, in the long wavelength limit, assuming potentials have radial symmetry, the scatterer is described by

$$\mathcal{V}_{\mathrm{ad}}(r) = \mathcal{V}_{\mathrm{SO}}(r) + V_0(r), \tag{1}$$

where $r = |\mathbf{r}|$, $\mathbf{r}$ being the charge carrier position. Thus, for $r \gg R$, where R is the range of the potential $\mathcal{V}_{\mathrm{ad}}$, the electronic wavefunction around the K point reads:

$$\psi_{\lambda,\mathbf{k},s}(\mathbf{r}) = \begin{pmatrix} 1 \\ \lambda \end{pmatrix} e^{ikr\cos\theta}|s\rangle + \frac{f^{ss}(\theta)}{\sqrt{-ir}} \begin{pmatrix} 1 \\ \lambda e^{i\theta} \end{pmatrix} e^{ikr}|s\rangle + \frac{f^{s\bar{s}}(\theta)}{\sqrt{-ir}} \begin{pmatrix} 1 \\ \lambda e^{i\theta} \end{pmatrix} e^{ikr}|\bar{s}\rangle\ , \tag{2}$$

where $\lambda = \pm 1$ indicates the carrier polarity (electron or hole) with energy $\epsilon = \lambda\hbar v_F k$, the ket $|s = \pm\rangle$ describes the orientation of the spin along the z-axis, perpendicular to the graphene plane ($\bar{s} \equiv -s$); $f^{ss}(\theta)$ and $f^{s\bar{s}}(\theta)$ are the elastic and inelastic ('spin-flip') scattering amplitudes at scattered angle θ, respectively. The latter is related to the T-matrix satisfying the Lippmann-Schwinger equation, $\mathcal{T}(\epsilon) = \mathcal{V}_{\mathrm{ad}} + \mathcal{V}_{\mathrm{ad}}G_0(\epsilon)\mathcal{T}(\epsilon)$, where $G_0(\epsilon)$ is the Green's function whose Fourier transform reads $G_0(\epsilon) = (\epsilon - \mathcal{H}_0 + \lambda i0^+)^{-1}$. Thus, $f^{ss'}(\theta) = \langle\mathbf{k}s|\mathcal{T}(\epsilon)|\mathbf{p}s'\rangle$, $|\mathbf{k}| = k = |\mathbf{p}|$, and θ is such that $\cos(\theta) = \hat{\mathbf{p}}\cdot\hat{\mathbf{k}}$. Let us denote as $\mathcal{F}(\mathbf{k},\mathbf{p})$ the 4×4 matrix whose elements are $f^{ss'}(\theta)$ in the spin and valley subspace. We can use symmetries of the Hamiltonian $\mathcal{H} = \mathcal{H}_0 + \mathcal{V}_{\mathrm{ad}}$ to constraint the general form of the matrix $\mathcal{F}(\mathbf{k},\mathbf{p})$. In general, the 4×4 matrix $\mathcal{F}(\mathbf{k},\mathbf{p})$ is a linear combination of the 16 matrices $s_\alpha\tau_\beta$ where $\alpha, \beta = 0, x, y, z$ (where $\alpha = 0$ corresponds to the unit matrix and $\alpha = x, y, z$ to a Pauli matrix). However, the assumption of no intervalley scattering implies that $\mathcal{F}(\mathbf{k},\mathbf{p})$ commutes with $\tau_z s_0$. This reduces the set of matrices to $s_\alpha\tau_\beta$ where $\beta = 0, z$. If we further impose invariance under rotations about the axis perpendicular to the graphene plane, and time-reversal, we obtain

$$\begin{aligned}\mathcal{F}(\mathbf{k},\mathbf{p}) = {} & a s_0\tau_0 + b(\hat{\mathbf{k}}\wedge\hat{\mathbf{p}}) s_0\tau_z \\ & + c(\hat{\mathbf{k}}\wedge\hat{\mathbf{p}}) s_z\tau_0 + d s_z\tau_z \\ & + e_1\mathbf{n}_1\cdot\mathbf{s}\tau_0 + e_2(\hat{\mathbf{k}}\wedge\hat{\mathbf{p}})\,\mathbf{n}_2\cdot\mathbf{s}\tau_0 \\ & + f_1(\hat{\mathbf{k}}\wedge\hat{\mathbf{p}})\,\mathbf{n}_1\cdot\mathbf{s}\tau_z + f_2\mathbf{n}_2\cdot\mathbf{s}\tau_z.\end{aligned} \tag{3}$$

where the 2D vectors $\mathbf{n}_1 = \hat{\mathbf{k}} + \hat{\mathbf{p}}$ and $\mathbf{n}_2 = \hat{\mathbf{k}} - \hat{\mathbf{p}}$ form an *orthogonal* set and $\hat{\mathbf{k}}\wedge\hat{\mathbf{p}} = \sin\theta$. The functions a, b, c, d, e_i, f_i ($i = 1, 2$) are complex-valued functions of k and $\xi = \hat{\mathbf{k}}\cdot\hat{\mathbf{p}} = \cos\theta$. Note that e.g., for scatterers with intrinsic SOI, we can further require that the component of the spin perpendicular to the graphene plane (i.e., $\mathbf{s}\cdot\hat{\mathbf{z}} = s_z$) is conserved, which implies that $e_i = f_i = 0$. Thus, the terms proportional to e_i and f_i describe the spin-flip scattering. The symmetry constraints reflected in Eq. (3) can be used to show that, for an unpolarized incident beam of electrons, which is described by the density matrix $\rho_{\rm in} = \frac{1}{4}s_0\tau_0|\mathbf{k}\rangle\langle\mathbf{k}|$, the spin-flip components of the scattering amplitude do not contribute to the skew scattering cross section of a single scatterer. This result is also obtained for an ensemble of the model scatterer studied below, for which electron transport is described by the Boltzmann equation. The collision integral of the latter is determined by the matrix of elements of $\mathcal{F}(\mathbf{k},\mathbf{p})$.

We now briefly explain how the spin Hall effect is enhanced by a single scatterer through skew scattering mechanism, and the important role played by resonant impurities in graphene, as well as the main differences with a 2DEG. To this end, let us consider a scattering center inducing (locally) an intrinsic SOI i.e., $\Delta_I(r) \neq 0$. As remarked above, this type of SOI conserves s_z and therefore $f^{s\bar{s}}(\theta) = 0$. The details of the calculation of $f^{ss}(\theta)$ and the spin Hall angle are provided in the Supplementary Material (SM). Here it is sufficient to realize that owning to the structure of the spin-orbit coupling term $\Delta_I\tau_z\sigma_z s_z$ [$(\nabla V_0(r)\times\mathbf{p})\cdot\mathbf{s}$ in a 2DEG], SOI scatterers break micro-reversibility $|f^{ss}(\theta)| \neq |f^{ss}(-\theta)|$, giving rise to asymmetry in scattering events [c.f., terms proportional to $\hat{\mathbf{k}}\wedge\hat{\mathbf{p}}$ in Eq. (3)]. SOI still preserves time-reversal symmetry, which then favors up/down spins to scatter symmetrically around the incident direction $|f^{ss}(\theta)| = |f^{\bar{s}\bar{s}}(-\theta)|$, thus explaining the formation of a net spin Hall current as depicted schematically in Fig. 1. Indeed, at the level of a single scattering event, the skew cross section

$$I^s = \int_0^{2\pi} d\theta \sin\theta\, |f^{ss}(\theta)|^2\,, \tag{4}$$

is non-zero and has opposite signs for up/down spin orientations. A finite I_s is the hallmark of skew scattering. Clearly, the latter effect is absent in the first Born approximation, according to which the scattering amplitudes at angles $\pm\theta$ coincide and hence Eq. (4) is identically zero. Moreover, we found that, contrary to the case of a 2DEG, a non-perturbative treatment of the SOI potential $\mathcal{V}_{\rm SO}$ is in general required and that, in certain cases, the distorted wave Born approximation, which can be successfully used to treat SOI in the 2DEG [26, 32], fails to describe I_s correctly. A few examples illustrating the perturbative treatments and a discussion of their limitations in graphene are provided in the SM.

As a measure of asymmetry in scattering events we adopt the so-called transport skewness; for an intrinsic SOI scatterer, the latter is defined as $\gamma \equiv I^s/\sigma^s$, where $\sigma^s = \int d\theta(1-\cos\theta)\,|f^{ss}(\theta)|^2$ denotes the transport cross section for carrier with spin s [for Rashba SOI see discussion below Eq. (7)]. The exact evaluation of γ (see SM) shows that: (i) γ is generally non-zero for local SOIs of the intrinsic type, (ii) local Rashba SOIs induce $|\gamma| > 0$ provided that electron-hole symmetry is broken by a electrostatic term i.e., $V_0 \neq 0$, and (iii) $|\gamma|$ is maximum near at resonances in σ^s. To illustrate these findings, we take disk scatterers producing an uniform potential inside a disk of radius R (see Fig. 1), according to $\mathcal{V}_{\rm ad}(r) = (V_0 + \mathcal{V}_{\rm SO})\theta(r-R)$, with $\mathcal{V}_{\rm SO}$ being intrinsic or Rashba SOI with $\Delta_{I/R}(\mathbf{r}) \equiv \Delta$. In this work we take $\Delta \sim 10$ meV which is consistent with *ab initio* calculations for metal atoms absorbed in graphene [24, 35]. The skewness of SOI disk scatterers in the vicinity of a given resonance is shown in Fig. 2. The function $\gamma(V_0)$ is seen to follow a approximately symmetric (asymmetric) line-shape for intrinsic (Rashba) SOI with extrema. Note that γ tends to zero (non-zero) as $V_0 \to 0$ for a Rashba (intrinsic) SOI. We also found that γ is larger nearby sharp resonances, typically occurring at large V_0 (not shown). It is well-known that already small doses of certain adatoms with large effective V_0 values produce resonances near at the Fermi level of graphene [30] that might dominate transport (see Ref. [36] for transport measurements in graphene covered with hydrogen). For dilute SOI disorder, the parameter γ can therefore be seen as a figure of merit for the capability of generating net transverse spin currents via skew scattering from resonant impurities. In fact, as shown in what follows, in the absence of other sources of impurities and at zero temperature, the spin Hall angle equals the transport skewness. Crucially, the results in Fig. 2 show that a large V_0 is not a necessary condition to obtain large skewness.

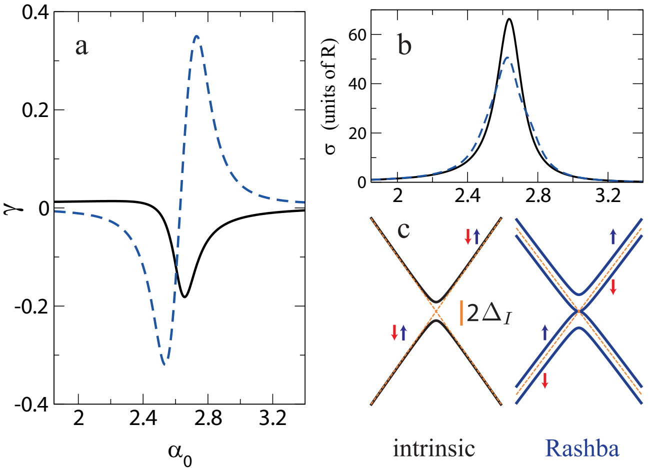

FIG. 2: Skew scattering induced by SOI impurities. (a) The skewness parameter $\gamma = I^s/\sigma^s$ as a function of α_0 for a SOI scatterer with range R of intrinsic (Rashba) type [solid black line (dashed blue line)]. Here $\alpha_0 \equiv V_0R/(\hbar v_F)$ characterizes the strength of the local electrostatic potential caused by the impurity. We have taken $kR = 0.15$ and SOI strength $\Delta R/(\hbar v_F) = 0.06$ (e.g., for $R = 4\,$nm these values correspond to $\hbar v_F k = 0.01\,$eV and $\Delta = 20\,$meV). Even larger values of γ can be found near sharper resonances (at larger V_0). (b) Transport cross section versus α_0 for the same parameters. The peaks corresponds to the first resonance for $V_0 > 0$. (c) Local band structure induced by SOI scatterers considered here. Dashed orange lines are guidelines to the eye representing the bulk band structure of monolayer graphene.

Although impurities such as H indeed induce giant effective potentials $V_0 \sim 10^2\,\mathrm{eV}$ (see Ref. [30] and references therein), we expect impurities leading to strong SOI couplings $\mathcal{V}_{\mathrm{SO}} \sim 10^2\,\mathrm{meV}$—needed to obtain a sizable γ—most likely produce effective V_0 values below those found for resonant scatterers such as H. These impurities could be heavy atoms or metal nano-particles that hybridize with p_z orbitals of graphene inducing relatively large local SOIs [22, 24].

After analyzing the SHE due to a single scatterer, we next turn to the experimentally relevant situation of dilute random ensemble of scatterers. To describe this situation, we need to solve the Boltzmann transport equations (BTEs), which for the steady state in the presence of a uniform electric field $\mathbf{E} = E\mathbf{e}_x$ read as [37]

$$\nabla_{\mathbf{k}} n_s(\mathbf{k}) \cdot (-e\lambda_{\mathbf{k}}\mathbf{E}) = \sum_{\mathbf{p},s'} W_{ss'}(\mathbf{k},\mathbf{p})\,[n_{s'}(\mathbf{p}) - n_s(\mathbf{k})]\ , \tag{5}$$

where $\lambda_{\mathbf{k}} = \mathrm{sign}(\epsilon_{\mathbf{k}})$ is the carrier polarity, $n_s(\mathbf{k})$ is the distribution function for spin s and $W_{ss'}(\mathbf{k},\mathbf{p}) \propto |f^{ss'}(\theta)|^2\,\delta(\epsilon_{\mathbf{k}} - \epsilon_{\mathbf{p}})$ with $\theta = \angle(\mathbf{k},\mathbf{p})$ is the quantum-mechanical scattering probability for processes with $\mathbf{k} \to \mathbf{p}$ and $s \to s'$. Notice that, skew scattering implies that $W_{ss'}(\mathbf{k},\mathbf{p}) \neq W_{ss'}(\mathbf{p},\mathbf{k})$ [c.f., Eq. (3)]. $W_{ss'}(\mathbf{k},\mathbf{p}) \equiv \sum_{\alpha=1}^{R} W^{(\alpha)}_{ss'}(\mathbf{k},\mathbf{p})$ takes into account all sources of disorder, where $R \geq 1$ is the number of such sources. The above BTEs can be solved exactly, within linear response theory, using the ansatz for $\delta n_s(\mathbf{k}) = n_s(\mathbf{k}) - n^0(\mathbf{k})$,

$$\delta n_s(\mathbf{k}) = \nabla_{\mathbf{k}} n^0(\mathbf{k}) \cdot [A_s(\mathbf{k}) e\mathbf{E} + B_s(\mathbf{k})\,(\hat{\mathbf{z}} \times e\mathbf{E})]\ , \tag{6}$$

where $n^0(\mathbf{k})$ is the Fermi-Dirac distribution. We determine $A_s(\mathbf{k})$ and $B_s(\mathbf{k})$ by solving Eq. (5) exactly in linear response. The charge and spin Hall currents follow from Eq. (6) according to $j_x = j_{x,\uparrow} + j_{x,\downarrow}$ and $j_{\mathrm{sH}} = j_{y,\uparrow} - j_{y,\downarrow}$, where $\mathbf{j}_s = -eg_v \sum_{\mathbf{k}} \delta n_s(\mathbf{k}) \lambda_{\mathbf{k}} v_{\mathbf{k}}$. Here, $g_v = 2$ stands for the valley degeneracy and $v_{\mathbf{k}} = (1/\hbar)\nabla_{\mathbf{k}}\epsilon_{\mathbf{k}}$. At zero temperature, the spin Hall angle $\theta_{\mathrm{sH}} \equiv j_{\mathrm{sH}}/j_x$ can be shown to assume the simple form

$$\theta_{\mathrm{sH}}|_{T=0} = \frac{\tau_{\parallel}}{\tau_{\perp}} = \bar{\gamma}\,, \tag{7}$$

where $\tau_{\parallel}^{-1} = \sum_{s',\mathbf{p}} (1 - ss'\cos\theta)\, W_{ss'}(\mathbf{k},\mathbf{p})$ and $\tau_{\perp}^{-1} = \sum_{\mathbf{p}} \sin\theta\, W_{ss}(\mathbf{k},\mathbf{p})$ are the transport scattering rate and skew scattering rate, respectively, evaluated at the Fermi energy ϵ_F. The spin Hall angle equals the *averaged* transport skewness $\bar{\gamma} = \bar{I}^s/\bar{\sigma}^s$ since $\bar{\sigma}^s \equiv \sum_\alpha v_F n_\alpha \sigma^s_\alpha = \tau_{\parallel}^{-1}$ and $\bar{I}^s \equiv \sum_\alpha v_F n_\alpha I^s_\alpha = \tau_{\perp}^{-1}$, where n_α is the impurity areal density from source α.

The relaxation rate has a distinct form in the spin-flip channel viz., $\tau^{-1}_{\parallel,\mathrm{flip}} = \sum_{\mathbf{p}} (1 + \cos\theta)\, W_{s\bar{s}}(\mathbf{k},\mathbf{p})$, and hence, for consistency, in the calculation of the skewness of a Rashba scatterer (Fig. 2), we have defined $\sigma^s \equiv \sum_{s'} \int d\theta (1 - ss'\cos\theta)|f^{ss'}(\theta)|^2$. We believe that the commonly employed definition, $\tau^{-1(\mathrm{approx.})}_{\parallel,\mathrm{flip}} = \sum_{\mathbf{p}} (1 - \cos\theta)\, W_{s\bar{s}}(\mathbf{k},\mathbf{p})$, is a spurious result of approximate treatments of transport equations; the relaxation rates defined here, on the other hand, result from the exact solution of the BTEs (in first order in $\mathbf{E}$). We also note that, for the type of potentials considered here, $W_{s\bar{s}} \propto |f_{s\bar{s}}(\theta)|^2$ is a function of $\cos(\theta)$, and thus the spin-flip amplitude does not contribute to $\tau_{\perp}^{-1}$. Further details of the solution and careful comparison with approximate treatments of the BTE will be reported elsewhere.

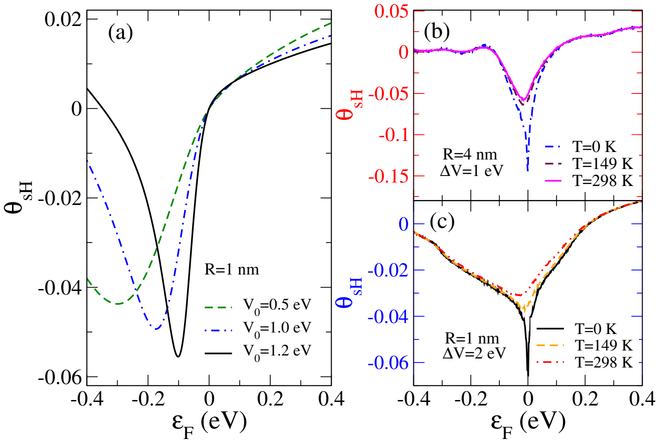

FIG. 3: Spin Hall angle as a function of Fermi energy for a dilute random distribution of intrinsic SOI scatterers. Panel a) shows θ_{sH} at zero temperature for impurities producing a (non-disordered) local electrostatic potential V_0. Panels b) and c) show θ_{sH} at differente temperatures and considering a random V_0 potential with uniform distribution $V_0 \in [0, \Delta V]$. In all panels we have taken $\Delta_I = 25$ meV.

Large SHEs are expected in relatively clean samples and when cross sections for unintentional sources of disorder are off resonance. In Fig. 3 [panels a), b) and c)] we show the spin Hall angle [Eq. (7)] as a function of Fermi energy for pristine graphene decorated with a small density of intrinsic SOIs (θ_{sH} induced by Rashba scatterers are of the same order of magnitude and hence are not shown). The values obtained are comparable with those found in metals $|\theta_{\mathrm{sH}}| \sim 0.01 - 0.1$ [5, 7, 12] and are robust with respect to thermal fluctuations and disorder averaging [compare curves in a) and c)]. Spin Hall angles of the order of 0.1 at room temperature are obtained for ‘fat scatterers’ with R of the order of a few nanometers [see panel b)]. We thus expect clusters of metals or nano-particles deposited in graphene to drive giant spin Hall currents. As a consistency check, we verified that the presence of a localized magnetic moment at the impurity does not supress the SHE when realistic values of the local exchange coupling are considered (see SM).

Conclusions. We have shown that fat scatterers—adatoms, molecules or nano-particles—inducing effective local spin-orbit couplings of intrinsic or Rashba type in a graphene sheet originate robust SHEs via assymetric (skew) scattering, with spin Hall angles comparable to state-of-the-art values for metals. The SHEs studied here are robust with respect to thermal fluctuations and disorder averaging. These findings suggest that functionalized graphene systems can be used to design spintronic integrated circuits with SHE-based spin-polarized current activation and control.

Acknowledgements. A.F. acknowledges support from National Research Foundation–Competitive Research Programme through award "Novel 2D materials with tailored properties: beyond graphene" (Grant No. R-144-000-295-281). T.G.R. acknowledges support from INCT - Nanocarbono, CNPq and FAPERJ. Discussions with N.M.R. Peres and A. Pachoud are greatly acknowledged.

[1] M. I. Dyakonov, and V. I. Perel, JETP Lett. **13**, 467 (1971).

[2] J. E. Hirsch, Phys. Rev. Lett. **83**, 1834 (1999).

[3] S. Zhang, Phys. Rev. Lett. **85**, 393 (2000).

[4] T. Jungwirth, J. Wunderlich, and K. Olejnik, Nature Mat. **11**, 382 (2012).

[5] Y. K. Kato, R. C. Myers, A. C. Gossard, and D. D. Awschalom, Science **306**, 1910 (2004).

[6] V. Sih, R. C. Myers, Y. K. Kato, W. H. Lau, A. C. Gossard, and D. D. Awschalom, Nature Phys. **1**, 31 (2005).

[7] K. Ando, and E. Saitoh, Nat. Commun. **3**, 629 (2012).

[8] S. O. Valenzuela, and M. Tinkham, Nature **442**, 176 (2006).

[9] T. Seki, Y. Hasegawa, S. Mitani, S. Takahashi, H. Imamura, S. Maekawa, J. Nitta, and K. Takanashi, Nature Mater. **7**, 125 (2008).

[10] L. Liu, T. Moriyama, D. C. Ralph, and R. A. Buhrman, Phys. Rev. Lett. **106**, 036601 (2011).

[11] L. Liu, C.-F. Pai, Y. Li, H. W. Tseng, D. C. Ralph, and R. A. Buhrman1, Science **336**, 555 (2012).

[12] M. Morota, Y. Niimi, K. Ohnishi, D. H. Wei, T. Tanaka, H. Kontani, T. Kimura and Y. Otani, Phys. Rev. B **83**, 174405 (2011).

[13] K. S. Novoselov, A. K. Geim, S. V. Morozov, D. Jiang, M. I. Katsnelson, I. V. Grigorieva, S. V. Dubonos, and A. A. Firsov, Nature **438**, 197 (2005); Y. Zhang, Y.-W. Tan, H. L. Stormer, and P. Kim, Nature **438**, 201 (2005); A. H. Castro Neto, F. Guinea, N. M. R. Peres, K. S. Novoselov, and A. K. Geim, Rev. Mod. Phys. **81**, 109 (2009).

[14] N. Tombros, C. Jozsa, M. Popinciuc, H. T. Jonkman, and B. J. van Wees, Nature **448**, 571 (2007).

[15] S. Cho, Y. F. Chen, and M. S. Fuhrer, Appl. Phys. Lett. **91**, 123105 (2007).

[16] W. Han, K. Pi, K. M. McCreary, Y. Li, J. J. I. Wong, A. G. Swartz, and R. K. Kawakami, Phys. Rev. Lett. **105**, 167202 (2010).

[17] A. Avsar, T.-Y. Yang, S. Bae, J. Balakrishnan, F. Volmer, M. Jaiswal, Z. Yi, S. R. Ali, G. Güntherodt, B. H. Hong, B. Beschoten, and B. Özyilmaz, Nano Lett. **11** 2363 (2011).

[18] B. Dlubak, M.-B. Martin, C. Deranlot, B. Servet, S. Xavier, R. Mattana, M. Sprinkle, C. Berger, W. A. De Heer, F. Petroff, A. Anane, P. Seneor, and A. Fert, Nature Physics **8**, 557 (2012).

[19] D. Huertas-Hernando, F. Guinea, and A. Brataas, Phys. Rev. B **74**, 155426 (2006).

[20] S. Konschuh, M. Gmitra, and J. Fabian. Phys. Rev. B **82**, 245412 (2010).

[21] D. Pesin, and A. H. MacDonald, Nature Materials **11**, 409 (2012).

[22] D. Marchenko, A. Varykhalov, M. R. Scholz, G. Bihlmayer, E. I. Rashba, A. Rybkin, A. M. Shikin & O. Rader. Nature Comm. **3**, 1232 (2012).

[23] A. H. Castro Neto, and F. Guinea, Phys. Rev. Lett. **103**, 026804 (2009).

[24] C. Weeks, J. Hu, J. Alicea, M. Franz, and R. Wu, Phys. Rev. X **1**, 021001 (2011).

[25] C. L. Kane, and E. J. Mele, Phys. Rev. Lett. **95**, 226801 (2005).

[26] V. V. Mkhitaryan, and M. E. Raikh, Phys. Rev. B **77**, 245428 (2008).

[27] A. C. Hewson, The Kondo Problem to Heavy Fermions (Cambridge Univ. Press, U.K., 1993).

[28] G.-Y. Guo, S. Maekawa, and N. Nagaosa, Phys. Rev. Lett. **102**, 036401 (2009).

[29] T. Stauber, N. M. R. Peres, and F. Guinea, Phys. Rev. B **76**, 205423 (2007); J. P. Robinson, H. Schomerus, L. Oroszlány, and V. I. Fal'ko, Phys. Rev. Lett. **101**, 196803 (2008). T. O. Wehling, S. Yuan, A. I. Lichtenstein, A. K. Geim, M. I. Katsnelson, Phys. Rev. Lett. **105**, 056802 (2010)

[30] A. Ferreira, J. Viana Gomes, J. Nilsson, E. R. Mucciolo, N. M. R. Peres, and A. H. Castro Neto, Phys. Rev. B **83**, 165402 (2011).

[31] J. Balakrishnan, G. K. W. Koon, M. Jaiswal, A. H. Castro Neto, and B. Özyilmaz, Nature Physics, doi:10.1038/nphys2576 (2013).

[32] L. E. Ballantine. Quantum Mechanics: A Modern Development (World Scientific, Singapore, 1998).

[33] T. G. Rappoport, B. Uchoa, and A. H. Castro Neto, Phys. Rev. B **80**, 245408 (2009).

[34] K. Pi, Wei Han, K. M. McCreary, A. G. Swartz, Yan Li, and R. K. Kawakami, Phys. Rev. Lett. **104**, 187201 (2010).

[35] J. Ding, Z. Qiao, W. Feng, Y.Yao, and Q. Niu, Phys. Rev. B **84**, 195444 (2011).

[36] J. Katoch, J.-H. Chen, R. Tsuchikawa, C. W. Smith, E. R. Mucciolo, and M. Ishigami, Phys. Rev. B **82**, 081417(R) (2010). Z. H. Ni, L. A. Ponomarenko, R. R. Nair, R. Yang, S. Anissimova, I. V. Grigorieva, F. Schedin, Z. X. Shen, E. H. Hill, K. S. Novoselov, A. K. Geim, Nano Lett. **10**, 3868 (2010)

[37] We have neglected spin-coherent part of the distribution function $n_s(\mathbf{k})$ and kept only the diagonal terms, which is expected to be a good approximation to describe transport at room temperature. Furthermore, in graphene, the BTE does not describe transport close to the Dirac point.

Supplementary Material

I. INTRINSIC SCATTERERS

The components of the graphene spinor $\Psi^{\pm}(\mathbf{r}) = (\psi_A^{\pm}(\mathbf{r}), \psi_B^{\pm}(\mathbf{r}))^T$ are decomposed in terms of radial harmonics: $\psi_A^{\pm}(\mathbf{r}) = \sum_{m=-\infty}^{\infty} g_{m,\pm}^{A}(r) e^{im\theta}$ and $\psi_B^{\pm}(\mathbf{r}) = \sum_{m=-\infty}^{\infty} g_{m,\pm}^{B}(r) e^{i(m+1)\theta}$ where $\theta_{\mathbf{k}}$ =arg$(k_x + ik_y)$ and

$k_x \pm ik_y = e^{\pm i\theta}(-i\partial_r \pm \frac{1}{r}\partial_\theta)$, where $m = 0, \pm1, \pm2, ...$ is the angular momentum quantum number, $\pm$ represents the spin projection and $A(B)$ denote the sublattice.

After separating the variables of the Hamiltonian $\mathcal{H}_0 + \mathcal{V}_{\rm ad} = v_F(\tau_z\sigma_x p_x + \sigma_y p_y) + \theta(r-R)[V_0 + \Delta_I \tau_z\sigma_z s_z]$, we obtain two coupled first order equations for the radial functions $g^A_{m,\pm}(r)$ and $g^B_{m,\pm}(r)$. Here, $\boldsymbol{\sigma}, \boldsymbol{\tau}$ and $\mathbf{s}$, are Pauli matrices acting on the sublattice, valley and spin degrees of freedom, respectively. Note that the spin-orbit interaction does not connect the states at different Dirac cones $\tau_z = \pm1$ and therefore each valley can be treated separately. Using the partial-waves expansion for spin-dependent scattering, the asymptotic form for the spinor wave function for an incoming wave-function with spin s at Dirac point K is given by

$$\psi_{\lambda,\mathbf{k},s}(\mathbf{r}) = \begin{pmatrix} 1 \\ \lambda \end{pmatrix} e^{ikr\cos(\theta)}|s\rangle + \frac{f^{ss}(\theta)}{\sqrt{-ir}} \begin{pmatrix} 1 \\ \lambda e^{i\theta_{\mathbf{k}}} \end{pmatrix} e^{ikr}|s\rangle + \frac{f^{s\bar{s}}(\theta)}{\sqrt{-ir}} \begin{pmatrix} 1 \\ \lambda e^{i\theta_{\mathbf{k}}} \end{pmatrix} e^{ikr}|\bar{s}\rangle\ , \tag{1}$$

where $\lambda = \pm1$ denotes the carrier polarity, $s = -\bar{s}$ and $f^{ss}(\theta)$ and $f^{s\bar{s}}(\theta)$ are the the scattering amplitudes without and with spin-flip, respectively.

Inside the disk ($r < R$), the eigenvalues of the Hamiltonian are given by $\epsilon \equiv E - V_0 = \lambda\sqrt{\hbar^2 v_F^2 k^2 + \Delta_I^2}$. Note that the spectrum has a gap of $2|\Delta_I|$. The problem is decoupled in spin and the two-component electron wave-function at valley K is

$$\psi_{\lambda,\mathbf{k},s}(\mathbf{r}) = \frac{1}{\sqrt{2\max(|\epsilon|, |\Delta_I|)}} \begin{pmatrix} \sqrt{\epsilon + s\Delta_I} \\ \eta\sqrt{\epsilon - s\Delta_I}e^{i\theta_{\mathbf{k}}} \end{pmatrix} e^{i\mathbf{k}\cdot\mathbf{r}}, \tag{2}$$

where $\eta = \mathrm{sgn}(\epsilon + |\Delta_I|)$. We can write the spinors for the region inside and outside the potential as a superposition of angular harmonics. For electrons in the region outside the disk ($r > R$), $E = \lambda\hbar v_F k$ and the partial wave m reads as

$$\psi_{\lambda,m,s}(r,\theta) = \begin{pmatrix} J_m(kr)e^{im\theta} \\ i\lambda J_{m+1}(kr)e^{i(m+1)\theta} \end{pmatrix} + S^s_m \begin{pmatrix} H^{(1)}_m(kr)e^{im\theta} \\ i\lambda H^{(1)}_{m+1}(kr)e^{i(m+1)\theta} \end{pmatrix}, \tag{3}$$

whereas for $r < R$ we have

$$\psi_{\lambda,m,s}(r,\theta) = C_m \begin{pmatrix} \sqrt{\epsilon + s\Delta_I}J_m(\beta r)e^{im\theta} \\ i\eta\sqrt{\epsilon - s\Delta}J_{m+1}(\beta r)e^{i(m+1)\theta} \end{pmatrix}, \tag{4}$$

where $\beta = \sqrt{\epsilon^2 - \Delta^2}/(\hbar v_{\rm F})$. The boundary condition at $r = R$ leads to two equations for each spin. The solution of these equations allow us to compute the amplitudes S^s_m. After some algebra, we obtain

$$S^s_m = -\frac{\sqrt{\epsilon + s\Delta_I}J_{m+1}(kR)J_m(\beta R) - \frac{\eta}{\lambda}\sqrt{\epsilon - s\Delta_I}J_{m+1}(\beta R)J_m(kR)}{\sqrt{\epsilon + s\Delta_I}H^{(1)}_{m+1}(kR)J_m(\beta R) - \frac{\eta}{\lambda}\sqrt{\epsilon - s\Delta_I}J_{m+1}(\beta R)H^{(1)}_m(kR)}. \tag{5}$$

The states with $|\epsilon| < \Delta_I$ correspond to damping waves since β is pure imaginary. It is straighfoward to show that the m-th phase-shift δ_m [3] relates to the amplitude S^s_m as defined in Eq. (3) according to $S^s_m = ie^{i\delta^s_m}\sin(\delta^s_m)$.

The Dirac equation for graphene in the presence of a scalar potential has a symmetry with respect to the exchange of g^A_m by g^B_{-m-1} which is responsible for the absence of backscattering. For $\mathcal{H}_I$, the symmetry is given by the exchange of $g^A_{m,\pm}$ by $g^B_{-m-1,\mp}$, which corresponds to a relation $\delta^\pm_{-m} = \delta^\mp_{m+1}$ between the spin-dependent phase-shifts. The $m = 0$ and $m = -1$ channels provide the main contributions for the spin dependent differential cross sections. If we consider the relation $\delta^\pm_{-m} = \delta^\mp_{m+1}$, we can write the scattering amplitudes in terms of the $m = 0$ channels for both spins: $f^s(\theta) = \sqrt{2/\pi k}(e^{i\delta^s_0}\sin\delta^s_0 + e^{i\delta^{-s}_0}\sin\delta^{-s}_0 e^{i\theta})$. The spin polarization is given by $P(\theta) = |f^+(\theta)|^2 - |f^-(\theta)|^2 = -(8/\pi k)\sin(\delta^+_0 - \delta^-_0)\sin(\theta)$, which is maximum for $\theta = \pm\pi/2$. These calculations can be performed in the other valley where $\tau_z = -1$. In fact, it is straightforward to show that the charge/spin conductivity tensor is the same in both valleys. Notice that taking into account both valleys of graphene, the Hamiltonian reads

$$\begin{aligned}\mathcal{H} &= v_F\left(\tau_z\sigma_x p_x + \sigma_y p_y\right) \\ &\quad + \left(V_0 + s\Delta_I\tau_z\sigma_z\right)\theta(r-R)\,,\end{aligned} \tag{6}$$

where $\tau_z = \pm1$ is the valley index and the above Hamiltonian acts on the space of spinorial functions in the form $\langle\boldsymbol{r}|\psi\rangle = \left(\Psi^K_A(\boldsymbol{r}), \Psi^K_B(\boldsymbol{r}), \Psi^{K'}_A(\boldsymbol{r}), \Psi^{K'}_B(\boldsymbol{r})\right)^T \otimes |\chi_s\rangle$. The effective Hamiltonian admits an even simpler representation if one swaps the K' components of the spinorial wavefunction. Indeed, defining $\langle\boldsymbol{r}|\tilde{\psi}\rangle = \left(\Psi^K_A(\boldsymbol{r}), \Psi^K_B(\boldsymbol{r}), \Psi^{K'}_B(\boldsymbol{r}), \Psi^{K'}_A(\boldsymbol{r})\right)^T \otimes |\chi_s\rangle$, we obtain an effective representation in the form of two copies of the Dirac Hamiltonian $\tilde{H}_0 = \hbar v_F\tau_z\boldsymbol{\sigma}\cdot\mathbf{p}$, plus a potential term with the same form in both valleys

$$V = \left(V_0 + s\Delta_I\sigma_z\right)\theta(r-R)\,. \tag{7}$$

The differential cross section is therefore the same for states in K and K' Dirac points.

II. TIME-REVERSAL SYMMETRY BREAKING SCATTERERS

Time-reversal symmetry is broken by local exchange fields. If we take an extra term in the Hamiltonian of the form $s\Delta_B\theta(r-R)$ where Δ_B is the local exchange field strength. Using the basis discussed in the previous section, with A and B sublattices swapped in the K' valley, we obtain

$$\begin{aligned}\tilde{\mathcal{H}} &= \tau_z v_F\left(\sigma_x p_x + \sigma_y p_y\right)\\ &\quad + \left(V_0 + s\Delta_I\sigma_z + s\Delta_B\right)\theta(r-R)\,,\end{aligned} \tag{8}$$

whose eigenvalues (inside the disk) are

$$\epsilon_s \equiv E - V_0 - s\Delta_B = \lambda\sqrt{{\Delta_I}^2 + \hbar^2 v_F^2 k^2}. \tag{9}$$

For electrons, the partial wave expansion for this problem is given by

$$\psi^e_{m,s}(r,\theta) = C_m\begin{pmatrix}\sqrt{\epsilon_s + s\Delta_I}\,J_m(\beta_s r)e^{im\theta}\\ i\tau_z\zeta_\tau\sqrt{\epsilon_s - s\Delta_I}\,J_{m+1}(\beta_s r)e^{i(m+1)\theta}\end{pmatrix}, \tag{10}$$

for $R < r$, and where $\zeta_\tau = \mathrm{sign}(\epsilon_s - |\Delta_I|)$. The momentum inside the disk depends on the spin orientation according to $\hbar v_F\beta_s = \sqrt{\epsilon^2_{s,\tau} - \Delta_I^2}$. For $r > R$, the wavefunction reads as

$$\begin{aligned}\psi^e_{m,s}(r,\theta) = &\begin{pmatrix}J_m(kr)e^{im\theta}\\ i\tau_z J_{m+1}(kr)e^{i(m+1)\theta}\end{pmatrix} +\\ &S_m^{s\tau}\begin{pmatrix}H_m^{(1)}(kr)e^{im\theta}\\ i\tau_z H_{m+1}^{(1)}(kr)e^{i(m+1)\theta}\end{pmatrix}.\end{aligned} \tag{11}$$

We verified that in general the exchange field does not destroy SHE even if Δ_B becomes comparable to other energy scales.

III. RASHBA SCATTERERS

If we consider a scatterer with a Rashba interaction, the diagonalization of the Hamiltonian $\mathcal{H}$ inside the disk ($r < R$) yields to eigenvalues $\epsilon_{\xi,s} = E_{\xi,s} - V = \xi\Delta_R + \lambda\sqrt{\hbar^2 v_F^2 k^2 + \Delta_R^2}$ where $\xi = \pm$ corresponds to the pseudospin degeneracy [1]. For simplicity we restrict the subsequent analysis to carriers with positive polarity (electrons), $\lambda = 1$, and assume $|\epsilon| > 2\Delta_R$. The eigenstates of $\mathcal{H}$ for the K cone can be written as

$$\psi^e_{\mathbf{k},s}(\mathbf{r}) = \left[\begin{pmatrix}1\\ \frac{\epsilon_{\xi,s}}{\hbar v_F k}e^{i\theta_\mathbf{k}}\end{pmatrix}|\uparrow\rangle + i\xi\begin{pmatrix}\frac{\epsilon_{\xi,s}}{\hbar v_F k}e^{i\theta_\mathbf{k}}\\ e^{2i\theta_\mathbf{k}}\end{pmatrix}|\downarrow\rangle\right]e^{i\mathbf{k}\cdot\mathbf{r}}. \tag{12}$$

Differently from the intrinsic SOI, Rashba SOI entangles spin and and pseudo spin, which means that s_z is not a good quantum number and spin-flips must be taken into account when calculating the scattering amplitudes ($f^{s,s'}(\theta) \neq 0$). In the case of scattering involving spin-flips, it is more convenient to work directly with partial-wave amplitudes. As before, we can write the eigenstates of the electrons for the region inside and outside the potential as a superposition of angular harmonics. For $r > R$ and a spin-up incident beam, the incoming and outgoing waves can be written as

$$\begin{aligned}\psi^e_{m,s}(r,\theta) = &\begin{pmatrix}J_m(kr)e^{im\theta}\\ iJ_{m+1}(kr)e^{i(m+1)\theta}\end{pmatrix}|\uparrow\rangle\\ &+ S_m^{\uparrow\uparrow}\begin{pmatrix}H_m^{(1)}(kr)e^{im\theta}\\ iH_{m+1}^{(1)}(kr)e^{i(m+1)\theta}\end{pmatrix}|\uparrow\rangle\\ &+ S_{m+1}^{\uparrow\downarrow}\begin{pmatrix}H_{m+1}^{(1)}(kr)e^{i(m+1)\theta}\\ iH_{m+2}^{(1)}(kr)e^{i(m+2)\theta}\end{pmatrix}|\downarrow\rangle.\end{aligned} \tag{13}$$

For $r < R$, the wave function regular at the origin can be written as the superposition

$$\begin{aligned}\psi^e_{m,s}(r,\theta) = \sum_\xi C_{\xi m}&\left[\begin{pmatrix}J_m(\beta_\xi r)e^{im\theta}\\ i\frac{\epsilon}{\hbar v_F\beta_\xi}J_{m+1}(\beta_\xi r)e^{i(m+1)\theta}\end{pmatrix}|\uparrow\rangle\right.\\ &\left.+\xi\begin{pmatrix}\frac{\epsilon}{\hbar v_F\beta_\xi}J_{m+1}(\beta_\xi r)e^{i(m+1)\theta}\\ iJ_{m+2}(\beta_\xi r)e^{i(m+2)\theta}\end{pmatrix}|\downarrow\rangle\right],\end{aligned} \tag{14}$$

where $\beta_\xi = \sqrt{\epsilon(\epsilon - 2\xi\Delta_R)}/\hbar v_F$. The matching conditions at $r = R$ give us four equations

$$J_m(kR) + S_m^{\uparrow\uparrow}H_m^{(1)}(kR) = \sum_\xi C_{\xi m}J_m(\beta_\xi R), \tag{15}$$

$$J_m(kR) + S_m^{\uparrow\uparrow}H_m^{(1)}(kR) = \sum_\xi C_{\xi m}J_m(\beta_\xi R), \tag{16}$$

$$S_m^{\uparrow\downarrow}H^{(1)}(kR) = \sum_\xi \xi\frac{\epsilon C_{\xi m}}{\hbar v_F\beta_\xi}J_{m+1}(\beta_\xi R), \tag{17}$$

$$S_m^{\uparrow\downarrow}H_{m+2}^{(1)}(kR) = \sum_\xi \xi C_{\xi m}J_{m+2}(\beta_\xi R). \tag{18}$$

We remark that Eq. (13) obeys the required boundary conditions. By taking a superposition of partial waves $\psi = \sum_m i^m\psi_m$ we obtain the asymptotic limit of the scattering solution of the Dirac equation in 2D:

$$\begin{aligned}\psi^e_{\mathbf{k},s}(\mathbf{r}) \to &\begin{pmatrix}1\\1\end{pmatrix}e^{ikr\cos\theta}|s\rangle\\ &+\sqrt{\frac{2}{i\pi kr}}\sum_{m=-\infty}^{\infty}S_m^{ss}e^{im\theta}\begin{pmatrix}1\\ e^{i\theta}\end{pmatrix}e^{ikr}|s\rangle\\ &+\sqrt{\frac{2}{i\pi kr}}\sum_{m=-\infty}^{\infty}S_m^{s\bar{s}}e^{im\theta}\begin{pmatrix}1\\ e^{i\theta}\end{pmatrix}e^{ikr}|\bar{s}\rangle\,,\end{aligned} \tag{19}$$

where we can identify the scattering amplitudes in the elastic and spin-flip channel as

$$f^{ss}(\theta) = \sqrt{\frac{2}{i\pi k}} \sum_{m=-\infty}^{\infty} S_m^{ss} e^{im\theta},$$

$$f^{s\bar{s}}(\theta) = \sqrt{\frac{2}{i\pi k}} \sum_{m=-\infty}^{\infty} S_m^{s\bar{s}} e^{im\theta}, \qquad (20)$$

respectively. The above expressions allow us to calculate the cross-sections used in the Boltzmann transport equation, namely the transport cross section and the skew cross section,

$$\sigma_{\text{transp}}^{ss'} = \int d\theta (1 - ss' \cos\theta) |f^{ss'}(\theta)|^2 , \qquad (21)$$

$$\sigma_{\text{skew}}^{ss'} = \int d\theta \sin\theta |f^{ss'}(\theta)|^2 , \qquad (22)$$

respectively. Inserting Eqs. (21)-(22) into the above expressions, we obtain the useful relations:

$$\sigma_{\text{transp}}^{ss'} = \frac{4}{k} \sum_{m=-\infty}^{\infty} |S_m^{ss'}|^2 - ss' \text{Re}[S_m^{ss'} (S_{m+1}^{ss'})^*] , \qquad (23)$$

$$\sigma_{\text{skew}}^{ss'} = \frac{4}{k} \sum_{m=-\infty}^{\infty} \text{Im}[S_m^{ss'} (S_{m+1}^{ss'})^*]. \qquad (24)$$

IV. DISTORTED WAVE BORN APPROXIMATION AND SHE IN GRAPHENE

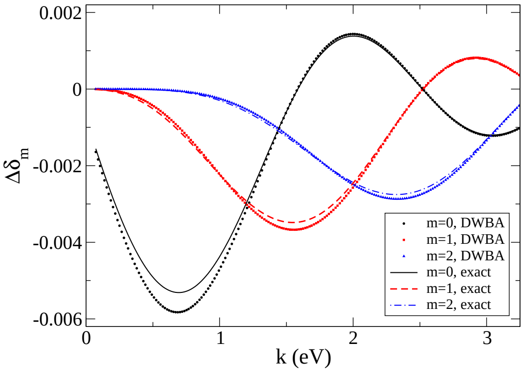

FIG. 1: Comparison between the exact value of $\Delta\delta_m = \delta_{V_0+\text{SO}} - \delta_{V_0}$ and DWBA approximation. The parameters are $\Delta_I s_z = 0.007$ eV, $V_0 = 0.07$ eV and $R = 1$ nm.

In this section, we provide a few examples of the limitations of the distorted wave Born approximation (DWBA) when applied to study spin Hall effect in graphene. We first derive the DWBA for a general class of potentials of the form

$$\mathcal{V}_a = V_a(r) + W_a(r)\sigma_z , \qquad (25)$$

where $W_a(r)$ denotes the sublattice symmetry breaking term. In analogy to the derivation for a scalar potential in the Schrödinger equation [2], it is necessary to write two copies of the Dirac equation corresponding to different potentials, V_1 and V_2. The scattering amplitudes (or phase-shifts, $\delta_m^{[1]}$) of the simpler problem $\mathcal{H}_1 \equiv \mathcal{H}_0 + \mathcal{V}_1$ are assumed to be known. Let us denote the eigenstates of $\mathcal{H}_a \equiv \mathcal{H}_0 + V_a$ by

$$\Psi_m^a(r, \phi) = e^{im\phi} \begin{pmatrix} F_a(r) \\ G_a(r)e^{i\phi} \end{pmatrix} , \qquad (26)$$

and $a = 1, 2$. We aim at finding the phase-shifts induced by the sublattice breaking term $W(r)$. Inserting the ansatz (26) into the Dirac equation, and using the asymptotic form of graphene wavefunctions

$$\Psi_m^a(r, \phi) \ \rightarrow \ \sqrt{\frac{2}{\pi k r}} \begin{bmatrix} \cos\left(kr - \lambda_m + \delta_m^a\right) \\ \lambda i \sin\left(kr - \lambda_m + \delta_m^a\right) \end{bmatrix} , \qquad (27)$$

we find

$$\frac{2\lambda}{\pi k} \sin\left(\delta_m^{[1]} - \delta_m^{[2]}\right) = \int_0^\infty drr \left[\frac{\delta\mathcal{V}_+}{\hbar v_F} F_1(r) F_2(r) - \frac{\delta\mathcal{V}_-}{\hbar v_F} G_1(r) G_2(r) \right] , \qquad (28)$$

where $\delta\mathcal{V}_\pm \equiv V_2 \pm W_2 - (V_1 \pm W_1)$. The above equation is still exact. The DWBA is derived by using the "Born approximation" $F_2(r) \simeq F_1(r)$ and $G_2(r) \simeq G_1(r)$. Specializing to the case of interest, i.e., $V_1 = V_2 = V_0(r)$, $W_1 = 0$, and $W_2 = W(r)$, the DWBA reads as

$$\Delta\delta_m = -\frac{\lambda\pi k}{2\hbar v_F} \int_0^\infty drr W(r) \left[f_m(r)^2 + g_m(r)^2 \right] , \qquad (29)$$

where $\Delta\delta_m = \delta_m^{[1]} - \delta_m^{[2]}$ is the correction to the m-th phase-shift $\delta_m^{[1]}$ introduced by the sublattice breaking term $W(r)$. In the above, $f_m(g_m)$ are the partial-wave amplitudes of the simpler problem $\mathcal{H}_1 = \mathcal{H}_0 + V_0(r)$, and $\lambda = \text{sgn}(E - V_0)$. We can use the equation above to calculate $\Delta\delta_m$ explicitly for a disk SOI scatterer with $V_0(r) = V_0\theta(r - R)$ and $W(r) = \Delta_I s_z \theta(r - R)$. In this case

$$\Delta\delta_m = -\frac{\lambda\pi k s_z}{2} \frac{\Delta_I k}{\hbar v_F \alpha^2} \int_0^{\alpha R} duu \left[J_m(u)^2 - J_{m+1}(u)^2 \right] . \qquad (30)$$

where $\alpha = |k - V/\hbar v_F|$. The above expression can be further simplified using the properties of Bessel functions (not shown). In Fig. 1 we can see the comparison between this approximation and the exact result.

The skew cross section can be easily calculated under the DWBA approximation:

$$\sigma_{\text{skew}}^{\text{DWBA}} = \frac{2}{k} \sum_{m=-\infty}^{\infty} (\Delta\delta_m - \Delta\delta_{m+1}) \cos[2(\delta_m^{[1]} - \delta_{m+1}^{[1]})]. \qquad (31)$$

The DWBA seems promising to compute phase-shifts for intrinsic SOI scatterer in the presence of a scalar potential. However, it fails to correctly describe the skew cross section (and thus SHE) for other symmetries or in the presence of resonant scattering. Here, we briefly discuss a few situations where the approximation is not valid. Our first example is provided by a void in graphene, which is described by the boundary condition requiring that the A-sublattice component of the spinor $\psi_{\lambda,\mathbf{k},s}(\mathbf{r})$ vanishes at $r = R$. Hence, the spin-independent part of the scattering phase shift $\delta_m^{[1]}$ fullfils:

$$\tan \delta_m^{[1]} = \frac{J_m(kR)}{Y_m(kR)}. \tag{32}$$

Note the symmetry $\delta_{-m}^{[1]} = \delta_m^{[1]}$. If we assume that the SOI potential only acts in the edge of the void i.e., $W(r) = R\Delta_I \delta(r-R)\tau_z\sigma_z s_z$, then, the DWBA yields:

$$\begin{aligned} \Delta\delta_m &\simeq \int rdr\ \Psi_m^\dagger(r,\phi) W(r) \psi_m(\Psi,\phi) \\ &= \Delta_I R \frac{[Y_m(kR)J_{m+1}(kR) - Y_{m+1}(kR)J_m(kR)]^2}{Y_m^2(kR)} \\ &\propto \Delta_I\,, \end{aligned} \tag{33}$$

where we have used the Wronskian identity for Bessel function, which implies that $Y_m(x)J_{m+1}(x) - Y_{m+1}(x)J_m(x) = 2/(\pi x)$. Hence, within the DWBA, $\delta_m^{[2]} = \delta_{-m}^{[2]}$, that is, the same symmetry as for the void potential, which implies the absence of skew scattering and therefore SHE.

A second example is provided by a generic Rashba scatterer, for which $W(r) = \Delta_R(r)\,(\tau^z\sigma^x s^y - \sigma^y s^x)$. It can be shown that within the DWBA, and at the lowest order in Δ_R, only the spin-flip amplitude $f^{s\bar{s}}(\theta) \neq 0$ gets corrected and therefore the skew cross section (and hence SHE) is zero in this approximation, just as in the previous example.

[1] D. Huertas-Hernando, F. Guinea, and A. Brataas, Phys. Rev. Lett. **103**, 146801 (2009).

[2] L. E. Ballantine. Quantum Mechanics: A Modern Development (World Scientific, Singapore, 1998).

[3] A. Ferreira, J. Viana Gomes, J. Nilsson, E. R. Mucciolo, N. M. R. Peres, and A. H. Castro Neto, Phys. Rev. B **83**, 165402 (2011).

[4] Notice that for a Rashba scatterer the DWBA derived earlier Eq. (29) does not apply.